Local structure around Er^{3+} in SiO_2-HfO_2 glassy waveguides using EXAFS

N. D. Afify and G. Dalba

Dipartimento di Fisica, Università degli Studi di Trento, Via Sommarive 14, I-38100 Povo (Trento), Italy

C. Armellini, M. Ferrari, and F. Rocca*

IFN-CNR, Istituto di Fotonica e Nanotecnologie del Consiglio Nazionale delle Ricerche,
Sezione FBK-CeFSA di Trento, Via alla Cascata 56/C, I-38100 Povo (Trento), Italy

A. Kuzmin

Institute of Solid State Physics, University of Latvia, LV-1063 RIGA, Latvia

Er^{3+}-doped SiO_2-HfO_2 glassy waveguides with HfO_2 concentrations ranging from 10 to 50 mol % were prepared using the sol-gel route and deposited on v-SiO_2 substrates using the dip-coating technique. The local environment around Er^{3+} ions was determined from Er L_3-edge extended x-ray-absorption fine-structure (EXAFS) measurements. The first coordination shell around Er^{3+} ions is composed of oxygen atoms. Hafnium is the main constituent of the second coordination shell of Er^{3+}, differing from the cases of pure SiO_2 and SiO_2-TiO_2 glassy hosts, in which silicon is the main atomic species. The local structure around Er^{3+} ions has been found to be independent on HfO_2 concentration within the studied composition range. This fact implies that Er^{3+} ions are preferentially dispersed in HfO_2-rich regions of the glassy waveguide, even at the lowest HfO_2 concentration. For all samples, no Er^{3+}-Er^{3+} coordination shell has been detected by EXAFS. The presented structural results allow us to understand some spectroscopic properties typical of Er^{3+}-doped SiO_2 glassy waveguides co-doped with HfO_2.

PACS number(s): 61.10.Ht, 78.66.Bz, 78.55.−m, 78.66.Jg

I. INTRODUCTION

Er^{3+}-activated SiO_2-based systems are important materials for standard telecommunication applications, since the $^4I_{13/2} \rightarrow {}^4I_{15/2}$ transition of the rare-earth Er^{3+} ion at a wavelength around 1.55 μm coincides with the lowest-loss window in the absorption spectra of SiO_2 glass based optical fibers.[1,2] For Er^{3+}-doped planar waveguide amplifiers (EDPWAs), the device dimensions should be as small as a few centimeters [integrated optics (IO) technology]. To achieve high gain in such tiny optical amplifiers, large concentrations of the rare-earth ion (Er^{3+}) should be homogeneously incorporated into the host glass, unlike the case of Er^{3+}-doped fiber amplifiers (EDFAs), in which the amplifier can be several meters long.

It is well-known that rare-earth ions tend to form chemical clusters (at short distances of few angstroms) and/or physical (or interaction) clusters (at large distances of 20–100 Å) at high concentrations.[3] The reason for that is to share oxygen atoms provided by the host glass, in order to compensate their own positive charge. It is believed that for the SiO_2 host, Er^{3+} ions are bound to nonbridging oxygen (NBO) atoms. It is also known that SiO_2 glass shows a quite low solubility for Er^{3+} ions. Consequently, at higher Er^{3+} contents, at least chemical clustering of Er^{3+} ions may occur. This gives rise to a quenching of the luminescence intensity by means of ion-ion interaction mechanisms.[3]

The sol-gel technique is a proper way to prepare rare-earth activated materials for photonics and optoelectronics applications. The most important features of this method are (i) the ability to homogeneously introduce rare-earth ions into a glassy host, (ii) tailoring of optical properties, and (iii) fabrication of planar waveguides as well as bulk glasses.[4]

It is widely accepted that the co-doping of the SiO_2 host with another oxide glass may increase the onset of rare-earth ion concentration quenching beyond the value typical of pure SiO_2 host. Such co-doping may also modify the local environment of the rare-earth ions, thus influencing the crystal-field dependent component of the luminescence process. Therefore the knowledge of detailed information on the local structure around the rare-earth ion is the key issue for selecting systems with optimized optical and spectral properties. One of the few tools that can monitor such local environment is the extended x-ray-absorption fine-structure (EXAFS) technique, since it is short-range-order (SRO) sensitive and element selective.

Many EXAFS studies on the local structure around Er^{3+} ions incorporated in SiO_2 glass co-doped with different oxides, having different chemical compositions, different heat treatments, as well as various preparation methods have been already reported in the literature. Rocca *et al.* studied Er^{3+}-doped SiO_2,[5,6] as well as SiO_2-Al_2O_3,[7,8] bulk glasses prepared by the sol-gel method, and SiO_2-TiO_2 glassy waveguides prepared by the same technique and deposited by dip coating.[8] Studies on (Yb^{3+}/Er^{3+})-doped SiO_2-TiO_2-Al_2O_3 glasses prepared by the sol-gel method were reported by D'Acapito *et al.*, either on bulk[9] or spin-coated waveguides.[10] The same authors studied also (Yb^{3+}/Er^{3+})-doped SiO_2 glasses containing silicon nanocrystals prepared by the ion implantation technique.[11] Marcus *et al.* described the local structure around Er^{3+} ions introduced into SiO_2 and SiO_2-Na_2O glassy films prepared by melting as well as by ion implantation techniques.[12] Er^{3+}-doped aluminosilicate and fluorosilicate prepared by melting were analyzed by Peters and Houde-Walter.[13,14] Mignotte reported

Er^{3+} local environments in pure TiO_2 and ZrO_2 layers prepared by sol-gel and deposited by dip-coating.[15,16]

The structure of Er^{3+}-doped SiO_2-based glasses has been also studied theoretically by means of molecular dynamics (MD). For example, Bernard *et al.* studied the structure of Er^{3+}-doped SiO_2-TiO_2.[17] MD results on Er^{3+}-doped SiO_2 as well as SiO_2-Na_2O glasses were also done by Jincheng and Cormack.[18,19]

These studies have led to some important conclusions about the effects of different co-dopant oxides on the local structure around the rare-earth ions hosted by SiO_2 glass. In most situations, the obtained structural information has been able to interpret the spectroscopic properties of such systems. To our knowledge, all the experimental and theoretical studies agree with the presence of about six oxygen atoms as the first nearest neighbors of Er^{3+}.

The results relative to the outer coordination shells around Er^{3+} ions are more interesting and system dependent, since they allow us to describe more deeply the different local environment of Er^{3+} in binary or ternary glassy hosts. In fact, the general outcome of these scientific investigations has allowed us to understand the roles of Al_2O_3, Na_2O, and TiO_2 oxides in Er^{3+}-doped SiO_2 glass. A common result of EXAFS studies is the absence of any Er^{3+}-Er^{3+} direct correlation, even at high concentrations of Er^{3+} and independently on the host co-dopant or its content. This suggests that any luminescence quenching might be originated from ion-ion interactions that are active at large Er^{3+}-Er^{3+} distances, well beyond the spatial resolution of the EXAFS technique.

Let us summarize the main conclusions reached on the roles of different SiO_2 glass co-dopants. For Al_2O_3 addition, it has been concluded that aluminium prefers to be present around Er^{3+} as substituent of silicon atoms. This conclusion was particularly stressed and clarified by Rocca *et al.* who reported that the addition of even small amounts of Al_2O_3 to SiO_2 host is able to modify the local structure around Er^{3+} ions, allowing for the incorporation of more Er^{3+} ions in SiO_2 without the occurrence of chemical clustering of the rare-earth ions.[7,8] Similar conclusions have been reported for Na_2O co-dopant.[12] For TiO_2 co-dopant,[8–10] the absence of titanium atoms from the local environment of Er^{3+} ions has been shown, in agreement with the fact that TiO_2 usually tends to be phase separated from the SiO_2 network.[20] For Er^{3+}-doped ZrO_2, the situation is not yet clear. Mignotte, who studied samples with Er^{3+} concentration as high as 15 mol %, ruled out the presence of erbium ions in zirconium sites, claiming the formation of erbium-rich clusters essentially different from the host matrix.[15,16] However, no clear attribution and modeling of the outer coordination shells around Er^{3+} ions, either in the amorphous or in the crystalline ZrO_2 host, was presented by the author.

From all these studies one can infer that the effect of SiO_2 co-dopant is to modify the local structure around Er^{3+} ions, which, however, remain still located mainly in the SiO_2 network.

In the present paper, we report on Er^{3+} ions hosted by another glassy system that shows new and different influence of the co-dopant of the SiO_2 host: SiO_2-HfO_2 glassy waveguides. Their local structure has been obtained by EXAFS measurements at the L_3-edge of Er. Waveguides containing HfO_2 concentrations ranging from 10 to 50 mol % have been investigated. Original findings about nearest and next-nearest neighbors of Er^{3+} ions have been found. The major result is the preferential presence of Er^{3+} ions in the co-dopant (i.e., HfO_2)-rich regions of the host glass, differing from all the previously studied SiO_2-based binary or ternary glassy hosts.

The paper is organized as follows. In Sec. II we describe the waveguide fabrication and EXAFS experiments. Sec. III is divided into two parts: in the first one, EXAFS data reduction and modeling procedures are illustrated; special attention is paid to the demonstration of accuracy of our analysis by reporting XRD and EXAFS results on crystalline Er_2O_3 reference compound; in the second part, the EXAFS results obtained on Er^{3+}-doped SiO_2-HfO_2 glassy waveguides are presented. The structural results are discussed and correlated to some spectroscopic properties in Sec. IV.

II. EXPERIMENTAL PROCEDURES

A. Samples preparation

Er^{3+}-doped SiO_2-HfO_2 glassy thin films with different HfO_2 contents (10, 20, 30, 40, and 50 mol %) were prepared following the sol-gel route. Henceforth, the five samples are denoted with the symbols W1, W2,… W5, consistently with the increasing HfO_2 concentration. The starting solution was obtained by mixing tetraethylorthosilicate (TEOS), ethanol (EtOH), deionized water (H_2O), and hydrochloric acid (HCl) as a catalyst. The $TEOS : HCl : H_2O$ molar ratio was of 1:0.01:2.0. Ethanolic colloidal suspension was prepared using hafnium oxychloride ($HfOCl_2 . 8H_2O$) as a precursor for hafnium. This solution was then added in different molar concentrations to the TEOS solution in order to have the required HfO_2 contents. Er^{3+} ions were introduced to the mixture solutions as erbium nitrates $[Er(NO_3)_3]$. The final mixture was stirred for 16 h at room temperature. The solution was then deposited on clean v-SiO_2 substrate using the dip-coating method,[21] with a dipping rate of 40 mm/min. Before further coating, each layer was heat treated at 900 °C in air for 55 s. After each ten dips, the film was heat treated at 900 °C for 2 min. The total number of dips was 20 for each sample, resulting in a final film thickness between 0.72 and 1.50 μm. Finally, the waveguides were further thermally treated at 900 °C for the minimum time required for a full densification of the film, carefully controlled as described in in Ref. 21. The final waveguides were of very good optical quality and crack-free. The absence of any crystalline phase was confirmed by x-ray diffraction. The nominal compositions, thicknesses, and heat treatments of the different waveguides are compiled in Table II.

Polycrystalline $ErVO_4$, used as a reference sample in EXAFS data analysis, was produced by chemical reaction of Er_2O_3 and V_2O_5. Stoichiometric amounts of these compounds were mixed and put together in an alumina crucible. The mixture was then heated at 680 °C for 12 h, cooled, ground, and heated again at 1000 °C for 12 h. XRD measurements have shown that the resulting product corresponds to tetragonal $ErVO_4$ (JCPDS card 170199).

B. EXAFS measurements

EXAFS measurements were carried out at the BM08 Beamline of ESRF, using the same conditions described in our previous works on Er³⁺-doped bulk glasses.[6,7] Er L_3-edge EXAFS spectra were collected at room temperature in fluorescence mode, since Er³⁺ concentrations were low and film thicknesses were of the order of 1 μm for all the investigated waveguides (for more details, see Table II). Fluorescence intensity was measured using a 13-element high purity Ge detector. The reference compounds ErVO₄ and Er₂O₃ (99.9% Aldrich) polycrystalline powders as well as 0.1-M Er nitrate hydrates aqueous solution [Er(NO₃)₃·5H₂O], needed for EXAFS data modeling, were measured in transmission mode. For each sample, 2–3 EXAFS spectra were collected to check the experimental data reproducibility. A portion of the same Er₂O₃ powder was also measured by x-ray diffraction, using X'PERT PRO diffractometer equipped with a Cu x-ray tube.

III. RESULTS

A. EXAFS data reduction

The raw x-ray-absorption spectra were aligned at the same photoelectron energy using the EXTRA code.[22] EXAFS data reduction was carried out using the EDA code.[23,24] For accurate best fit, the energy origin E_0 of the photoelectron energy should be determined for "unknown" and "reference" data. In our case, we used two sets of backscattering functions to select the correct position of the energy origin (see Sec. III B): (i) theoretical FEFF8 model and (ii) experimental Er nitrate hydrates aqueous solution. After some preliminary investigations, and following our previous experience, the origin of the photoelectron kinetic energy E_0 was set at the maximum of the white line for each experimental spectrum. This choice of E_0 gave very good agreement for both sets, and has been further confirmed by a best fit of the measured reference crystalline Er₂O₃ (see Sec. III B 1).

The pre-edge region was best fitted by a straight line in the energy range 8200–8330 eV. The atomiclike x-ray-absorption coefficient μ_o was obtained by best averaging the spectra with a polynomial function of the fourth degree in the energy range of 8400–9000 eV. The modulation of the absorption coefficient $\mu-\mu_o$ was normalized to μ_o in order to obtain the local structure-dependent part of the x-ray-absorption spectra $\chi(k)=(\mu-\mu_o)/\mu_o$.

Figure 1 reports the experimental EXAFS spectra of the different waveguides: EXAFS signals weighted by k [i.e., $k\chi(k)$] are shown in Fig. 1(a), and the moduli of their Fourier transforms $|F(R)|$ are reported in Fig. 1(b). In the interval 0.8–3.3 Å, $|F(R)|$ shows a major peak at about 1.7 Å and a contribution at about 2.9 Å. These structures can be attributed to the first two coordination shells around Er³⁺ ions, as well as to multiple-scattering effects. Our analysis has demonstrated that the multiple-scattering contribution is negligible, and that the structures in the range 0.8–3.3 Å [Fig. 1(b)] are due to the first shell Er³⁺-O pair correlation and second shell Er³⁺-Hf pair correlation, respectively. In the following, the modeling procedure of these two coordination shells is described.
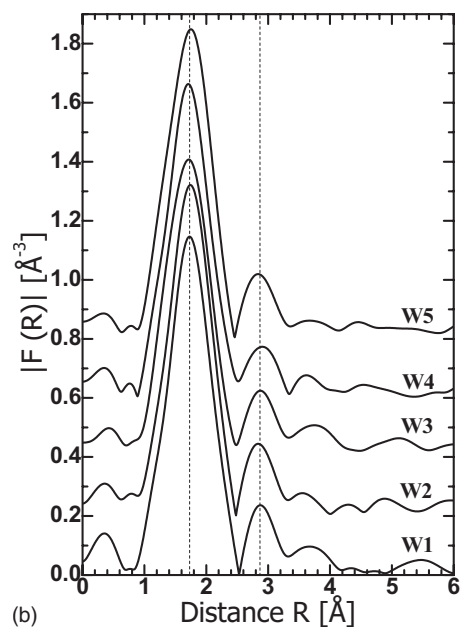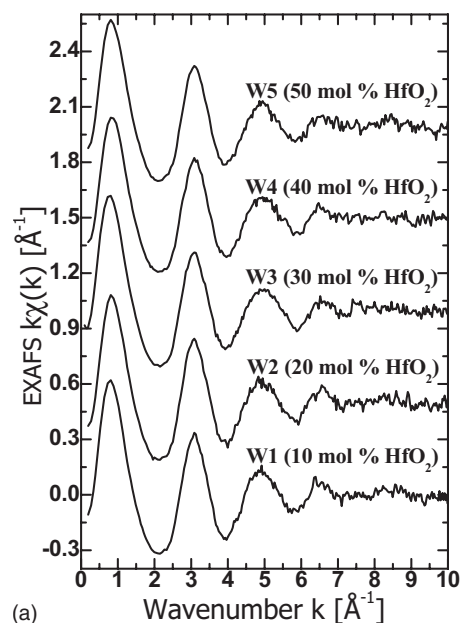
FIG. 1. Er L_3-edge EXAFS spectra of Er³⁺-doped SiO₂-HfO₂ waveguides at different concentrations of HfO₂ (see Table II for details). Spectra are vertically shifted for clarity. (a) EXAFS signals $k\chi(k)$. (b) Fourier transforms moduli of the EXAFS signals $k^2\chi(k)$. The k^2 weight will be used in all the following figures.

B. EXAFS data modeling

EXAFS signals were modeled employing the EDA code[23,24] on the basis of the usual multishell fitting procedure

$$\chi(k) = \sum_i \frac{N_i}{kR_i} F_i(k,R_i) \times \exp[-2\sigma_i^2 k^2]\sin[2kR_i + \Phi_i(k,R_i)],$$

(1)

where i labels the coordination shells, N_i is the coordination number, R_i is the average interatomic distance, σ_i is the

(a)

(b)
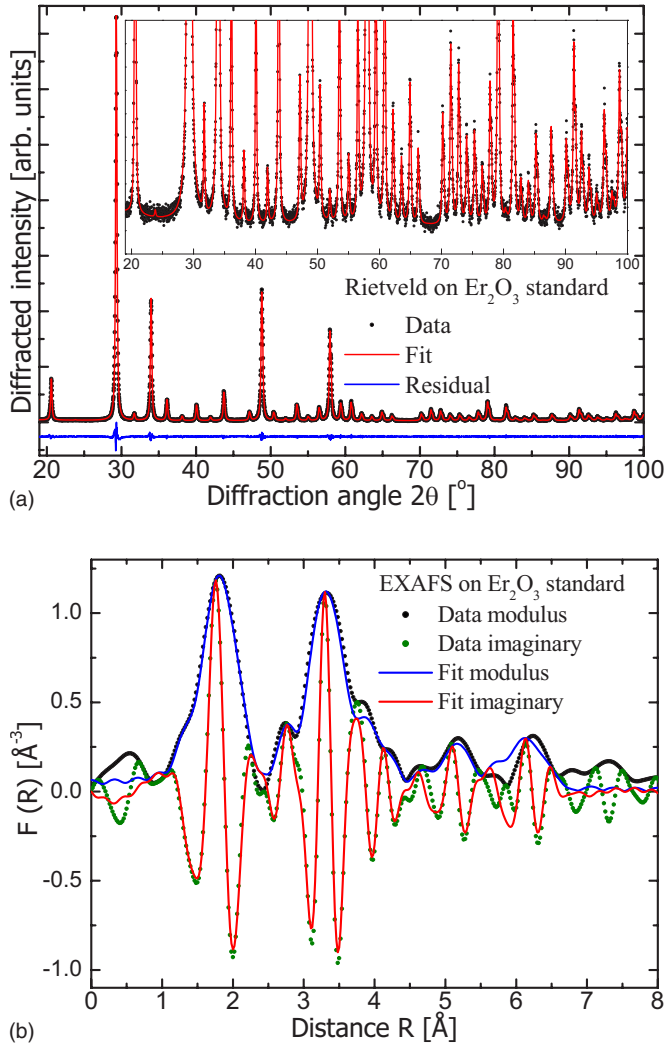
FIG. 2. (Color online) XRD and EXAFS results of crystalline Er$_2$O$_3$ reference compound. (a) Observed and Rietveld-refined x-ray-diffraction patterns and their difference. (b) Experimental and calculated Fourier transform of EXAFS signal $k^2\chi(k)$.

mean-square relative displacement or Debye-Waller exponent. The scattering amplitude $F_i(k, R_i)$ includes all nonstructural effects such as the damping due to the mean free path of the photoelectron and the S_0^2 amplitude scaling factor due to multi-electron effects. $\Phi_i(k, R_i)$ is the total scattering phase shift, including both central and neighboring atoms. The best fits were performed on the original experimental EXAFS signals $k^n\chi(k)$ (with $n = 1, 2, 3$ depending on the situation as described in the following), without any previous filtering of the nearest or next-nearest shell contributions. This procedure allowed us to exclude errors in the separation of the peaks in the Fourier transforms $|F(R)|$ of different experimental spectra, and to eliminate the effects of Fourier and back-Fourier filtering in a limited range. The ability of the Gaussian approximation to reproduce the first shell of Er in the studied waveguides was also checked: as documented in Fig. 3(b) the quality of best fits is so high both for real and imaginary parts of the $F(R)$ that any additional asymmetry parameter would be only a source of additional uncertainty in the quantitative results.

TABLE I. Parameters of the local structure around Er^{3+} ions in the reference crystalline compound Er$_2$O$_3$ extracted from the L_3-edge of Er. N, R, and σ^2 are the coordination number, average interatomic distance, and Debye-Waller disorder factor, respectively. Numbers in parentheses are the numerical uncertainties on the last digits. The interatomic distances geometrically calculated from the refined crystallographic model R_{XRD} are also reported for comparison.

Coordination shell	N (atom)	R (Å)	σ^2 (Å^2)	R_{XRD} (Å)
Er^{3+}-O	6	2.281(5)	0.0083(6)	2.263
Er^{3+}-Er^{3+} (1)	6	3.509(2)	0.0039(3)	3.496
Er^{3+}-Er^{3+} (2)	6	3.987(5)	0.0062(5)	3.980
Er^{3+}-Er^{3+} (3)	6	5.30(1)	0.009(1)	5.275
Er^{3+}-Er^{3+} (4)	12	6.32(2)	0.009(6)	6.329

To fit EXAFS signals, the backscattering phase and amplitude functions of different atomic pair correlations were extracted experimentally resorting to reference compounds, or calculated using the FEFF8 code.[25,26] For the first coordination shell, both experimental and theoretical backscattering functions could be used in the modeling process. The theoretical ones were calculated and optimized starting from the structure of Er$_2$O$_3$ crystal that was refined by the present authors. The experimental backscattering functions were extracted from the EXAFS signal at the Er L_3-edge of Er nitrate hydrates aqueous solution, where an isolated Gaussian distribution is expected. Note that a best fit of this EXAFS signal using theoretical functions has been able to reproduce almost perfectly the structural parameters reported in Ref. 27. For the second coordination shell (Er^{3+}-Hf), only the theoretical functions calculated starting from the ErVO$_4$ crystal structure (by replacing V by Hf in the FEFF8 calculations[6]) were used, due to the difficulty to single out the second shell contribution from the experimental data.

1. Results of crystalline Er$_2$O$_3$ reference compound

In order to check the accuracy of the backscattering amplitudes and phase shifts functions, and to demonstrate the reliability of our EXAFS analysis on the waveguides, we report here the results obtained for the crystalline Er$_2$O$_3$ reference powders, whose structure has been carefully refined by XRD before the EXAFS experiments and data analysis.

The crystallographic model corresponding to the body-centered-cubic Er$_2$O$_3$ lattice (ICSD card no. 39185) has been refined via Rietveld fitting procedure using the general structure analysis system GSAS code.[28] Figure 2(a) reports the observed X-ray diffraction pattern, the Rietveld-refined one, and their difference. From the magnified portion in the inset of the same figure, the high quality of Rietveld best fit can be deduced. The refined value of the lattice parameter a is equal to 10.551 ± 0.001 Å, in good agreement with the value reported in the mentioned ICSD card (10.550 Å). The geometrically calculated average interatomic distances for some coordination shells around Er^{3+} ions are reported in Table I.

EXAFS spectra of the same Er$_2$O$_3$ powder compound were modeled using the EDA code. For the Er^{3+}-O first co-

ordination shell, the experimental backscattering functions mentioned above were used, while for the successive Er³⁺-Er³⁺ correlations, we used the amplitude and phase shift calculated theoretically by the FEFF8 code starting from crystalline ErVO₄ structure. The experimental EXAFS signals $k^2\chi(k)$, without any Fourier filtering, were fitted to the first five coordination shells in the k range 2.5–12.5 Å⁻¹. Each coordination shell was represented by three parameters (N, R, σ^2), assuming Gaussian radial distribution functions around the absorber atom, with the coordination numbers constrained to their crystallographic values for all correlations. The energy origin E_0 was fixed for all coordination shells. We assumed that oxygen atoms located in the outer coordination shells around Er³⁺ give negligible contributions to EXAFS with respect to the ones provided by the heavy Er³⁺ atoms. No multiple-scattering terms were included in the fit in order to avoid their correlation with the single-scattering path parameters. In spite of these limitations, a high best-fit quality parameter has been found, as depicted also by Fig. 2(b), which documents in the real space the very good reproduction of the real and imaginary parts of the Fourier transform. The structural parameters obtained from the best fit of Fig. 2(b) for the first five coordination shells are presented in Table I, in which the distances refined from x-ray-diffraction data on the same powders of Er₂O₃ are also reported for comparison. From this table, the good agreement between EXAFS and XRD results is evident. This validates also our choice for the E_0 position, because five coordination shells are correctly reproduced.

2. Results of Er³⁺-doped SiO₂-HfO₂ waveguides

After having verified the goodness of the used backscattering functions and the reliability of our analysis procedure for a well characterized crystalline reference, we may enter now in the analysis of the results obtained for the unknown Er³⁺-doped waveguides. The least-square fitting of the EXAFS signals $k^2\chi(k)$ has been performed using the same weighting factor $n=2$ applied to Er₂O₃. The only difference is in the fitted k range, that was 1.5–7.5 Å⁻¹. As it is evident from Fig. 1(a), EXAFS signals have a good quality at least up to 7.5 Å⁻¹ for all the studied samples; the data beyond this region have not been considered in the final fit because of the insufficient S/N ratio. For all spectra, the energy origin E_0 was fixed during the fits. The results of the best-fit procedure in reciprocal and real spaces for the first two coordination shells Er³⁺-O and Er³⁺-Hf are shown in Fig. 3. In Fig. 3(a), the experimental (empty circles), best-fit (red curve), Er³⁺-O (green curve), Er³⁺-Hf (blue curve), and residual (black curve) EXAFS signals $k^2\chi(k)$ are reported for two waveguides containing the lowest, 10 mol %, and the largest, 50 mol %, concentration of HfO₂. The k_{max} =9.5 Å⁻¹ shown in Fig. 3(a) is higher than the one we have applied in the final analysis (7.5 Å⁻¹) just to show the ability of this two-shell combination to reproduce frequencies at high k values although they are covered by noise. In Fig. 3(b), the experimental moduli and imaginary parts of the EXAFS Fourier transforms of the different waveguides are compared with the calculated ones. For the first coordination shell (Er³⁺-O), the fit was repeated using other experimental

(a)

(b)
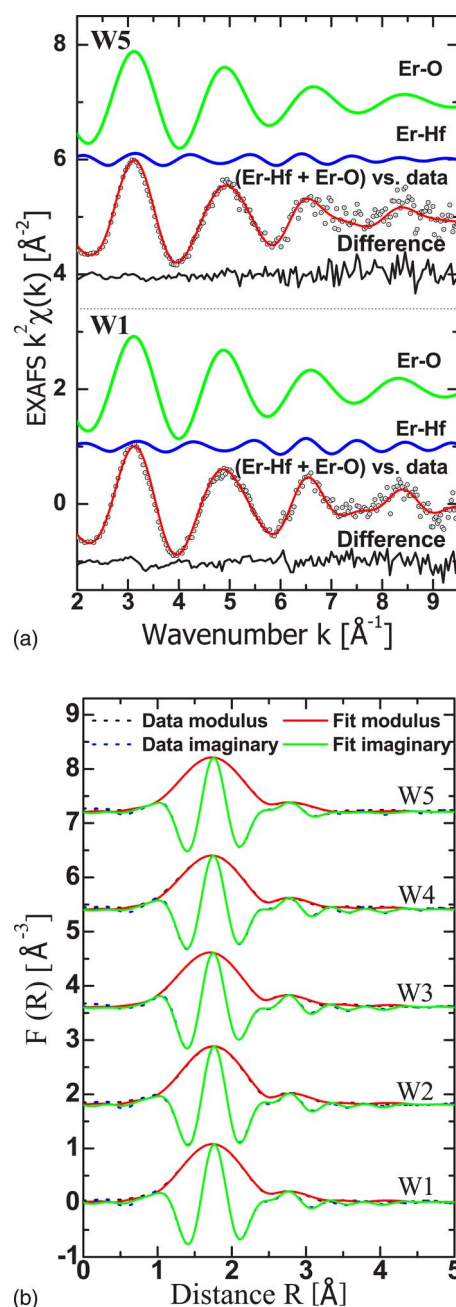
FIG. 3. (Color online) Modeling results of Er L_3-edge EXAFS signals $k^2\chi(k)$ of different waveguides. Spectra are vertically shifted for clarity. (a) Spectra of the waveguides containing the lowest 10% W1, and the largest, 50%, W5, with the molar concentration of HfO₂, respectively, are shown. Experimental (empty circles), best-fit (red-curve), Er³⁺-O (green curve), Er³⁺-Hf (blue curve), and residual (black curve) EXAFS signas $k^2\chi(k)$. (b) Experimental and best-fit calculated Fourier transforms of the $k^2\chi(k)$ EXAFS signals.

and theoretical backscattering functions based on the structure of Er₂O₃ reference compound. The best fit in this case was of comparable quality. The obtained structural parameters have been found reproducible in the different cases. The structural parameters of the first and the second coordination shells are reported in Table II. It should be noted that the reported coordination numbers, interatomic distances,

TABLE II. Nominal compositions, thicknesses, heat treatments, and the structural parameters of the first and second coordination shells of Er^{3+} in SiO_2-HfO_2 glassy waveguides with different HfO_2 contents. N, R, and σ^2 are the average coordination number, interatomic distance, and Debye-Waller factor, respectively. Numbers in parentheses are the estimated uncertainty on last digit taking into account different best fits.

Waveguide label		W1	W2	W3	W4	W5
HfO_2 content (mol %)		10	20	30	40	50
Er^{3+} content (mol %)		0.3	0.3	0.5	0.3	0.3
Thickness (micron)		1.500	1.280	0.690	0.960	0.722
Heat treatment time at 900°		30 hr	3.5 hr	5 min	5 min	2 min
First coordination	N (atom)	5.1(1)	5.1(1)	4.8(1)	5.0(2)	4.9(2)
shell	R (Å)	2.34(1)	2.33(1)	2.34(2)	2.33(2)	2.33(1)
(Er^{3+}-O)	σ^2 (Å^2)	0.011(2)	0.012(2)	0.012(2)	0.013(2)	0.012(2)
Second coordination	N (atom)	4.0(7)	3.9(7)	3.4(1)	3.8(2)	4.9(9)
shell	R (Å)	3.51(1)	3.52(1)	3.51(1)	3.50(1)	3.53(2)
(Er^{3+}-Hf)	σ^2 (Å^2)	0.015(4)	0.013(4)	0.011(2)	0.014(4)	0.020(9)

and Debye-Waller factors are the values averaged over the different backscattering functions as well as the various best-fitting procedures.

It is important to compare the Er^{3+}-O first coordination shell distance obtained in this work as well as in our previous studies[6–8] to the ones reported in literature by various authors. In Ref. [10], D'Acapito *et al.* reported the Er^{3+}-O distance of 2.25–2.27 Å in the SiO_2-TiO_2-Al_2O_3 system, depending on the content of Al_2O_3 in the host glass. These values are much shorter than the ones obtained by us: 2.32 Å in Er^{3+}-doped SiO_2; 2.33–2.35 Å in Er^{3+}-doped SiO_2-Al_2O_3 (slightly depending on Al_2O_3 content); and 2.34 Å in Er^{3+}-doped SiO_2-TiO_2. In a second paper on the same system, the same authors reported an Er^{3+}-O distance of 2.31–2.32 Å, by collecting EXAFS data at the Er K-edge.[9] These last distances are similar to the distances obtained by us from EXAFS spectra collected at Er L_3-edge. Peters *et al.* in Ref. [14] obtained the distance of 2.22 Å in 1 mol % Er^{3+}-doped SiO_2. In Ref. [12], Marcus *et al.* reported the distance of 2.28 Å in 0.3 at. % Er^{3+}-doped SiO_2. Still shorter interatomic distances have been reported using molecular-dynamics simulation. Bernard *et al.* in Ref. [17] obtained an Er^{3+}-O distance of 2.2 Å in Er^{3+}-doped SiO_2-TiO_2. This distance was independent on either Er^{3+} (0.7–1.5 mol %) or TiO_2 (7.8–15.7 mol %) concentrations. Cormack *et al.* in Ref. [18] obtained an Er^{3+}-O distance of 2.17 Å in 1 mol % Er^{3+}-doped SiO_2. This distance increased to 2.2 Å for Er^{3+} content of 5 mol %. In a following paper,[19] Cormack *et al.* reported an Er^{3+}-O distance of 2.19 Å in 1 mol % Er^{3+}-doped SiO_2. This distance increases on the addition of Na_2O to the glass up to 2.24 Å for a system with 30 mol % Na_2O. From this review, it is evident that significantly different values have been obtained for the Er^{3+}-O distances in the literature, but it is not easy to attribute the differences to real structural modifications or to data analysis procedures. The reliability of the data reported in the present work relies not only on the agreement with our previous results,[5–8] but mainly on the fact that the utilized analysis and modeling procedures have been carefully tested providing a very good

agreement with the x-ray-diffraction data for the reference crystalline Er_2O_3 material up to the fifth coordination shell.

Before discussing the results we give now more details about the attribution of the second coordination shell to the Er^{3+}-Hf correlation. As a matter of fact, one of the most important issues in modeling process is the attribution of the outer coordination shells to the correct atomic pair correlations. This is particularly critical when the contribution to the EXAFS signal of the second shell is weak in comparison with the first one as in the present case, where it is represented by the contribution at 2.9 Å of the Fourier transform modulus $|F(R)|$ [Fig. 1(b)]. The attribution of the Er^{3+} second shell to Hf atoms has been facilitated by the double-peak shaped backscattering amplitude, typical of heavy atoms as Hf, that is very different from that of oxygen and silicon and also distinguishable (in the best-fitting procedures) from that of Er. In order to verify the results presented in this paper, we have also explored some alternative scenarios, comparing various fitting strategies on the whole set of samples. At first, we fitted the experimental data by assuming that the second coordination shell of Er^{3+} was alternatively constituted by O, or Si or Er atoms. None of these three coordinations was able to reproduce the full EXAFS signal with the best-fit quality parameter comparable with the one given by Er-Hf coordination [Figs. 3(a) and 3(b)]. The absence of detectable Er-Er correlations confirms our previous studies.[7,8] As for the expected presence of Si in the second shell of Er, it was not accepted not only for the poor best-fit quality parameters, but also for the instability of quantitative results obtained from different best-fitting procedures and for the different samples.

A second more complex test was done: at first the unfiltered EXAFS signals of all the experimental spectra were best fitted to the contribution of the first shell (Er^{3+}-O), and the obtained signals were subtracted from the experimental data. Next, the second shell signal was extracted for each spectrum from the residuals by Fourier filtering procedure. The reliability of the resulting signals was evaluated by comparing different spectra collected for the same sample: some

spectra were thus excluded from the next quantitative step. The resulting isolated second shell signals were tested for Er^{3+}-O, Er^{3+}-Si, Er^{3+}-Er^{3+}, and Er^{3+}-Hf pair correlations. Once again, only in the case of Hf ions was the best fit of sufficiently good quality. This means, in summary, that only the Er-Hf correlations are sufficiently reproducible and ordered in the waveguides to give rise to a recognizable signal, even though of low intensity. As expected for an amorphous system, the high degree of disorder strongly reduces the EXAFS signal of the next-nearest neighbors of Er: the possible presence of other species in addition to Hf is not detectable with certitude by EXAFS on the basis of the present experimental data.

IV. DISCUSSION

In the following, the structural results extracted from the EXAFS spectra are discussed in relation with some spectroscopic properties of the system. From EXAFS data, we have deduced the presence of oxygen and hafnium as the nearest and next-nearest neighbor of erbium, respectively. While the identification of the first shell around Er^{3+} ions was expected, the one of the second shell was not taken for granted. For all previously studied Er^{3+}-doped SiO$_2$ based glasses, silicon has been always suggested as the main constituent of the second coordination sphere of the rare-earth ion; only in the case of Al-co-doping we were able to monitor little changes of the local structure around Er^{3+} in SiO$_2$ glass.[7,8] Therefore the present case shows a different role of the co-dopant oxide. We consider the identification of Hf as the main constituent of the second coordination shell around Er^{3+} as the most important result of this work.

At first, let us discuss the results on the first coordination shell around Er^{3+} ions, summarized in Table II. Within the estimated error bars, the structural parameters of the first coordination shell do not depend on the HfO$_2$ (10–50 mol %) or Er^{3+} (0.3–0.5 mol %) concentrations. Not only the distances, but also the coordination numbers and Debye-Waller factors are almost constant for all the samples. The distance is slightly longer than in the case of pure silica waveguides; the coordination number evaluated by EXAFS is lower than 6, as in previous studies on rare-earth-activated silicate glasses.[6–8] We should remember that this is an average information: it results from structural disorder, due to local deformations of bond distances and from the presence of different Er sites in the amorphous network. EXAFS data indicate the presence of a distorted octahedral environment for Er^{3+}, as suggested previously also by the authors of Ref. 29.

Next we are going to discuss the results obtained for the second coordination shell of Er^{3+} ions. The structural parameters compiled in Table II imply that EXAFS detects in the second coordination shell four to five hafnium atoms at an average radius of 3.51±0.02 Å, still independent on Er^{3+} or HfO$_2$ molar concentrations. It is worthwhile to note that the Er^{3+} second shell distance for the current system is shorter than the ones found in glasses without HfO$_2$ (for example, the Er^{3+}-Si distance is 3.74±0.01 Å in 0.2 mol % Er^{3+}-doped SiO$_2$). This result makes once again the
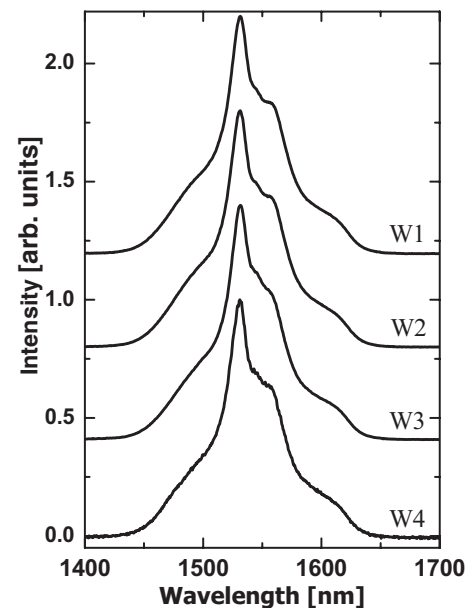
FIG. 4. Room-temperature photoluminescence (PL) spectra relative to the $^4I_{13/2} \rightarrow {}^4I_{15/2}$ transition of Er^{3+} ions incorporated in W1, W2, W3, and W4 waveguides. The PL spectra were obtained upon excitation at 514.5 nm (Ref. 30). Spectra from different waveguides are vertically shifted for clarity.

SiO$_2$-HfO$_2$ host a particular system, where the crystal field around the rare-earth ion is modified with respect to the one in pure silica glass.

On the basis of the presence of hafnium ions in the second coordination shell of Er^{3+}, we assume that Er^{3+} ions are dispersed in vitreous HfO$_2$-rich regions of the waveguide. Moreover, the finding that the structural parameters of the Er^{3+}-Hf second coordination shell do not depend on Er^{3+} (0.3–0.5 mol %) or HfO$_2$ (10–50 mol %) concentrations indicates that even at the lowest HfO$_2$ concentrations, Er^{3+} ions are preferentially dispersed in the regions rich of HfO$_2$. This result agrees with an analogous finding obtained for the same waveguides by Raman spectroscopy:[30] the structure of the glass in presence of hafnia was found to be strongly modified with respect to the case of pure SiO$_2$, remaining unchanged for all the studied HfO$_2$ concentrations (10–40 mol %). In Ref. 30 Ferrari and co-workers pointed out the strong similarity among the photoluminescence (PL) spectra (the PL spectra of some of the current waveguides, as extracted from Ref. 30, are reported in Fig. 4), showing that the Er^{3+} luminescence properties are independent on HfO$_2$ concentration. The authors interpreted the experimental results on the assumption that hafnium ions are coordinated to more than four oxygen atoms, with the consequent creation of nonbridging oxygen (NBO) atoms[31] in the silica network. The presence of NBOs results in a "network flexibility" that allows the host silica glass to accommodate Er^{3+} ions in almost equivalent environments.[32] In their model, HfO$_2$ was considered able to slightly modify the silica host glass structure so as to facilitate the dispersion of higher contents of Er^{3+} ions.

However, our results focus the attention to a different perspective: in our opinion it is the presence of hafnium in the

second coordination shell of Er^{3+} ions the key issue to understand the structural and spectroscopic properties. Photoluminescence spectra and shortened lifetimes can be explained by considering that the incorporation of HfO_2 in silica strongly modifies the next-nearest shell environment around Er^{3+}, inducing an increase of the electric dipole component of the $^4I_{13/2} \rightarrow {}^4I_{15/2}$ transition probability. The independence of the luminescence process on the HfO_2 content ranging from 10 to 40 mol % means that the crystal-field-dependent component of the luminescence process remains unchanged. This is equivalent to say that the local structure around Er^{3+} remains unchanged. Therefore the reported EXAFS results explain very well the strong similarity among the observed PL spectra of the different waveguides. The independence of the Er^{3+} local environment on Er^{3+} concentration (0.3 and 0.5 mol %), as has been found by EXAFS measurements, allows us also to explain why SiO_2-HfO_2 is able to host more Er^{3+} ions beyond the quenching limit of SiO_2.[33]

V. CONCLUSIONS

In this paper, the detailed local structure around Er^{3+} ions incorporated in SiO_2-HfO_2 glassy waveguides has been investigated by EXAFS technique. The first coordination sphere around Er^{3+} is composed of five to six oxygen atoms at an average interatomic distance of 2.33 Å. Hafnium is the main atomic species present in the second coordination shell. Both the first and the second coordination shells of Er^{3+} ions are independent on HfO_2 (10–50 mol %) and Er^{3+} (0.3–0.5 mol %) concentrations. These results indicate that Er^{3+} is preferentially dispersed in HfO_2-rich regions of the waveguide, already at the lowest concentrations of HfO_2. The reported results are able to explain some spectroscopic properties of these waveguides.

On the basis of the current EXAFS results and the previous PL ones, HfO_2 co-doping yields two effects: (i) an increase of Er^{3+} solubility in the host glass, and (ii) modification of the crystal field around Er^{3+}, keeping it unchanged for a wide range of HfO_2 concentrations.

*rocca@science.unitn.it

[1] W. Miniscalco, J. Lightwave Technol. **9**, 234 (1991).

[2] *Rare Earth Doped Fiber Lasers and Amplifiers*, edited by M. Digonnet (Marcel Dekker, New York, 2001).

[3] E. Desurvire, *Erbium-Doped Fiber Amplifiers: Principles and Applications* (J. Wiley and Sons, Inc., New York, 1994).

[4] R. Almeida *et al.*, Philos. Mag. **84**, 1659 (2004).

[5] F. Rocca, F. Monti, A. Kuzmin, A. Dalmaso, and D. Pasqualini, J. Synchrotron Radiat. **6**, 737 (1999).

[6] F. Rocca, C. Armellini, M. Ferrari, G. Dalba, N. Diab, A. Kuzmin, and F. Monti, J. Sol-Gel Sci. Technol. **26**, 267 (2003).

[7] F. Rocca, M. Ferrari, A. Kuzmin, N. Daldosso, C. Duverger, and F. Monti, J. Non-Cryst. Solids **293-295**, 112 (2001).

[8] N. Afify, R. Grisenti, G. Dalba, C. Armellini, M. Ferrari, S. Larcheri, F. Rocca, and A. Kuzmin, Opt. Mater. (Amsterdam, Neth.) **28**, 864 (2006).

[9] F. D'Acapito, S. Mobilio, L. Santos, and R. Almeida, Appl. Phys. Lett. **78**, 2676 (2001).

[10] F. D'Acapito, S. Mobilio, P. Gastaldo, D. Barbier, F. Santos, O. Martins, and R. Almeida, J. Non-Cryst. Solids **293-295**, 118 (2001).

[11] C. Maurizio, F. D'Acapito, F. Priolo, G. Franzó, F. Iacona, E. Borsella, S. Padovani, and P. Mazzoldi, Opt. Mater. (Amsterdam, Neth.) **27**, 900 (2005).

[12] M. Marcus and A. Polman, J. Non-Cryst. Solids **136**, 260 (1991).

[13] P. Peters and S. Houde-Walter, Appl. Phys. Lett. **70**, 541 (1997).

[14] P. Peters and S. Houde-Walter, J. Non-Cryst. Solids **239**, 162 (1998).

[15] C. Mignotte, J. Non-Cryst. Solids **291**, 56 (2001).

[16] C. Mignotte, Appl. Surf. Sci. **226**, 355 (2004).

[17] C. Bernard, S. Chaussedent, A. Monteil, and M. Ferrari, Philos.

Mag. B **82**, 681 (2002).

[18] D. Jincheng and A. Cormack, Radiat. Eff. Defects Solids **157**, 789 (2002).

[19] D. Jincheng and A. Cormack, J. Non-Cryst. Solids **351**, 2263 (2005).

[20] R. Almeida, J. Sol-Gel Sci. Technol. **13**, 51 (1998).

[21] R. Gonçalves, G. Carturan, L. Zampedri, M. Ferrari, M. Montagna, A. Chiasera, G. Righini, S. Pelli, S. Ribeiro, and Y. Messaddeq, Appl. Phys. Lett. **81**, 28 (2002).

[22] P. Fornasini and F. Rocca, EXTRA, software for EXAFS data analysis, University of Trento, 1998.

[23] A. Kuzmin, Physica B **208-209**, 175 (1995).

[24] A. Kuzmin and J. Purans, J. Phys.: Condens. Matter **12**, 1959 (2000).

[25] J. Rehr, J. Mustre de Leon, S. Zabinsky, and R. Albers, J. Am. Chem. Soc. **113**, 5135 (1991).

[26] J. Mustre de Leon, J. J. Rehr, S. I. Zabinsky, and R. C. Albers, Phys. Rev. B **44**, 4146 (1991).

[27] H. Ohtaki and T. Radnai, Chem. Rev. (Washington, D.C.) **93**, 1157 (1993).

[28] A. Larson and R. V. Dreele, Los Alamos National Laboratory Report LAUR No. 86, 2000 (unpublished).

[29] M. Ishii and Y. Komukai, J. Appl. Phys. **94**, 2368 (2003).

[30] L. Zampedri *et al.*, J. Non-Cryst. Solids **345-346**, 580 (2004).

[31] D. Neumayer and E. Cartier, J. Appl. Phys. **90**, 1801 (2001).

[32] S. Todoroki, K. Hirao, and N. Soga, J. Appl. Phys. **72**, 5853 (1992).

[33] R. Gonçalves, G. Carturan, M. Montagna, M. Ferrari, L. Zampedri, S. Pelli, G. Righini, S. Ribeiro, and Y. Messaddeq, Opt. Mater. (Amsterdam, Neth.) **25**, 131 (2004).